HHS Public Access

Author manuscript

Chromosome Res. Author manuscript; available in PMC 2017 June 07.

Published in final edited form as:

Chromosome Res. 2015 June ; 23(2): 171–186. doi:10.1007/s10577-014-9444-6.

Comparative cytogenetic characterization of primary canine melanocytic lesions using array CGH and fluorescence in situ hybridization

Kelsey Poorman,
Department of Molecular Biomedical Science, College of Veterinary Medicine, North Carolina State University, 1060 William Moore Drive, Raleigh, NC 27607, USA

Luke Borst,
Department of Pathobiology and Population Health, College of Veterinary Medicine, North Carolina State University, Raleigh, NC, USA

Scott Moroff,
Antech Diagnostics, 1111 Marcus Avenue, Lake Success, NY, USA

Siddharth Roy,
Department of Statistics, College of Physics and Applied Mathematics, North Carolina State University, Raleigh, NC, USA

Philippe Labelle,
Antech Diagnostics, 1111 Marcus Avenue, Lake Success, NY, USA

Alison Motsinger-Reif, and
Department of Statistics, College of Physics and Applied Mathematics, North Carolina State University, Raleigh, NC, USA, Center for Comparative Medicine and Translational Research, North Carolina State University, Raleigh, NC, USA

Matthew Breen
Department of Molecular Biomedical Science, College of Veterinary Medicine, North Carolina State University, 1060 William Moore Drive, Raleigh, NC 27607, USA, Center for Comparative Medicine and Translational Research, North Carolina State University, Raleigh, NC, USA, Cancer Genetics Program, UNC Lineberger Comprehensive Cancer Center, Chapel Hill, NC, USA

Abstract

Melanocytic lesions originating from the oral mucosa or cutaneous epithelium are common in the general dog population, with up to 100,000 diagnoses each year in the USA. Oral melanoma is the most frequent canine neoplasm of the oral cavity, exhibiting a highly aggressive course. Cutaneous melanocytomas occur frequently, but rarely develop into a malignant form. Despite the differential prognosis, it has been assumed that subtypes of melanocytic lesions represent the same disease. To address the relative paucity of information about their genomic status, molecular cytogenetic

Correspondence to: Matthew Breen.

Electronic supplementary material The online version of this article (doi:10.1007/s10577-014-9444-6) contains supplementary material, which is available to authorized users.

analysis was performed on the three recognized subtypes of canine melanocytic lesions. Using array comparative genomic hybridization (aCGH) analysis, highly aberrant distinct copy number status across the tumor genome for both of the malignant melanoma subtypes was revealed. The most frequent aberrations included gain of dog chromosome (CFA) 13 and 17 and loss of CFA 22. Melanocytomas possessed fewer genome wide aberrations, yet showed a recurrent gain of CFA 20q15.3–17. A distinctive copy number profile, evident only in oral melanomas, displayed a sigmoidal pattern of copy number loss followed immediately by a gain, around CFA 30q14. Moreover, when assessed by fluorescence in situ hybridization (FISH), copy number aberrations of targeted genes, such as gain of c-*MYC* (80 % of cases) and loss of *CDKN2A* (68 % of cases), were observed. This study suggests that in concordance with what is known for human melanomas, canine melanomas of the oral mucosa and cutaneous epithelium are discrete and initiated by different molecular pathways.

Keywords

Canine; Oral melanoma; Cytogenetics; Array; Comparative; genomic hybridization

Introduction

Melanocytes are highly motile melanin-producing cells, usually found in the basal layer of the epidermis. The primary function of these cells is to protect the nuclei of neighboring epithelial cells from UV damage, yet they can also give rise to both benign melanocytomas and malignant melanomas. In dogs, melanomas are the most common tumor of the oral cavity, 90 % of which are malignant, readily invading into normal tissue and bone, with a high metastatic propensity (Ramos-Vara et al. 2000; Koenig et al. 2002; Spangler and Kass 2006; Bergman 2007). Malignant melanomas of the oral cavity are usually aggressive and respond poorly to standard-of-care chemotherapeutic treatments (Bergman 2007). Melanomas of the cutaneous epithelium are the third most common malignant skin lesion in dogs (Villamil et al. 2011) representing 5–11 % of all malignant melanomas (Smith et al. 2002). There is also a debate among veterinary pathologists concerning the accuracy of prognostic criteria for canine malignant melanomas (Withrow et al. 2013).

Numerous retrospective studies have correlated survival with physical characteristics of the tumor, including anatomical site, gender, volume of tumor, and also with histological parameters, such as pigmentation and mitotic index (Ramos-Vara et al. 2000; Overly et al. 2001; Kudnig et al. 2003; Spangler and Kass 2006). In a study of 122 canine melanocytic tumors, mitotic index and location, classical markers of malignancy, were not significantly correlated with survival time (Ramos-Vara et al. 2000). A subsequent study of 384 cases of melanocytic tumors found a significant correlation of metastasis, mitotic index, nuclear atypia, WHO clinical stage, and volume with decreased patient survival (Spangler and Kass 2006). However, the same study also found that only 59 % of cases determined to be histologically malignant exhibited biological malignancy (metastasis or recurrence). It was also determined that 74 % of tumors of ‘ambiguous location’ (feet or lips) were reported malignant via histology, yet only 38 % of these demonstrated malignant behavior. Finally, of the 227 presumed benign melanocytic skin lesions, 39 % were reported as histologically

malignant, with 12 % exhibiting malignant behavior (Spangler and Kass 2006). This lack of uniformity demonstrates the need for more accurate diagnostic and prognostic markers for affected canine patients.

Cytogenetic studies of human melanomas have revealed that the underlying genetic mutations associated with these lesions differ significantly depending on the location of the primary tumor (Curtin et al. 2005; Blokx et al. 2010; Furney et al. 2012; Thomas et al. 2014). It is now believed that these lesions are initiated from and subsequently develop through molecularly different pathways, reflecting the variation in therapeutic response (Bastian et al. 2003; Bauer and Bastian 2006). Cytogenetic studies also identified specific DNA copy number aberrations correlating with tumor malignancy, which have allowed for sensitive diagnostic and prognostic assays to be developed (Bauer and Bastian 2006). Assays have been developed using both fluorescence in situ hybridization (FISH) (Gaiser et al. 2010) and array-based comparative genomic hybridization (aCGH) techniques (Furney et al. 2013). Such cytogenetic studies have also allowed for the discovery of novel genes and pathways leading to targeted therapeutics (Xie et al. 2012).

Recent developments in the field of veterinary and comparative oncology have made it possible to characterize tumors through genome-wide molecular cytogenetic analysis (Breen 2009). Genome-wide studies expedite the discovery of novel mutations and facilitate the development of both molecular markers and targeted therapies with the ultimate goal to obtain better clinical outcome. Previous investigations have identified important cancer-related proteins in the pathogenesis of canine oral melanoma (Ritt et al. 1998; Koenig et al. 2002; Bianco et al. 2003; Newman et al. 2011). In parallel to the observations in human studies, it has been hypothesized that dysregulation of comparable genes in dogs may be a function of aberrant gene dosage and/or functional translocation (Xie et al. 2012). However, no study has investigated the role of copy number aberrations in canine melanocytic lesions.

To address the lack of information in this field, the goal of this study was to characterize cytogenetic changes evident in canine melanocytic lesions, using oligonucleotide array comparative genomic hybridization array (oaCGH) and multicolor fluorescence in situ hybridization (FISH), and to assess the comparative value of these data by consideration of features shared with subtypes of human melanomas.

Materials and methods

Clinical specimens

Canine oral melanomas and benign melanocytomas were obtained with informed owner consent, as biopsy specimens from patients undergoing a routine diagnostic procedure. Samples were selected randomly with no prior knowledge of diagnostic parameters. A formalin-fixed paraffin-embedded (FFPE) specimen of each case was evaluated by a veterinary pathologist during initial diagnosis. Where the diagnostic hematoxylin and eosin (H&E) slide was made available (56/67 cases), the initial diagnosis was independently confirmed by three further board certified veterinary pathologists (SM, PL, and LB) and assessed for percent pigmentation, mitotic index, presence of junctional activity, and tissue morphology as previously described (Smedley et al. 2011). Differences in histologic

characteristics between melanomas and benign melanocytomas were analyzed for statistical significance with a two-tailed Mann–Whitney *U* Test.

The cohort for DNA isolation was comprised of specimens from 67 individuals; 53 were available to the study only as the fixed tissue specimen, 11 were available only as a snap frozen tumor punch biopsies, and 3 were available as both FFPE and snap frozen tumor tissue. The cases used for DNA isolation were comprised of 44 biopsies of primary oral melanomas either FFPE (n=32) or fresh frozen (n=12), 5 biopsies of cutaneous melanomas either FFPE (n=3) or fresh frozen (n=2), and 18 FFPE biopsies of primary cutaneous melanocytoma. All unfixed tumor specimens (punch biopsies) were snap frozen in liquid nitrogen at the time of removal and subsequently stored at −80 °C. A direct comparison of copy number profiles from fresh tissue and the corresponding tumor-enriched FFPE sample showed no difference in called aberrations, indicating that punch biopsies were not substantially infiltrated with non-neoplastic cells (SOM Fig. 1). As such the study used both snap frozen punch biopsies and FFPE derived specimens as the source of tumor DNA. A detailed description of the specimens used in the study is provided in Table 1.

Genomic DNA extraction

Genomic DNA was extracted from tumor punch biopsies using the Qiagen DNeasey Kit according to the manufacturer's recommendations (Qiagen, German-town, MD, USA) and assessed for quality and quantity by spectrophotometry. Genomic DNA integrity, assessed by agarose gel electrophoresis, indicated little to no degradation.

Within the cohort of FFPE samples, several contained inked margins with bordering non-neoplastic tissue. To avoid DNA from these non-neoplastic regions being present in the experimental sample, areas of tissue enriched for tumor were identified on a representative H&E-stained 5 μm slide by two veterinary pathologists (PL and LB). Three adjacent 25 μm sections were then obtained from each FFPE specimen and the non-neoplastic tissue was macro-dissected away. Genomic DNA was extracted from the remaining neoplastic regions using a Qiagen DNA Removal for FFPE Samples kit, according to manufacturer's recommendations (Qiagen, Germantown, MD, USA), and subsequently assessed for quality and quantity by spectrophotometry. Genomic DNA integrity was assessed by agarose gel electrophoresis, indicating that while all FFPE derived specimens exhibited some degree of degradation, the majority of the DNA was >10 kb.

Fluorescence in situ hybridization of archival specimens

FISH was performed to detect and quantify target genomic regions, using 5 μm FFPE sections of the cases in the cohort. Each 5 μm FFPE section was mounted onto a charged glass slide and incubated at 56 °C for 18 h in a moisture-free slide chamber. Slides were then dewaxed by soaking in fresh xylene for 15 min, dehydrated through an ethanol series, and air-dried. Slides were incubated for 1 h at 37 °C in 60 mg/mL collagenase II (Sigma, Saint Louis, MO) in HBSS (Mediatech, Corning, NY) and then for 45 min at 37 °C in Tris-Buffer Saline (Boston BioProducts, Boston, MA) containing 15,000 unit/mL of Bovine Testicular Hyaluronidase (Sigma, Saint Louis, MO). Slides were rinsed with ultra pure water for 3 min

between treatments. Sections were then treated with an Abbott Paraffin Pre-treatment Kit II according to the manufacturer's recommendation.

Tissue slices were assessed by FISH to evaluate the copy number of canine bacterial artificial chromosome (BAC) probes representing ten genes, selected to correspond to those identified by previous human studies of melanoma; *CDKN2A*, *CDKN1A*, *PTEN*, *B-RAF*, *TP53*, *CCND1*, *c-MYC*, *c-KIT*, *CDK4*, and *RB-1*. The BACs were selected from the CHORI-82 (https://bacpac.chori.org/library.php?id=253) library based on their genome position indicated in the USCS canine genome browser (http://genome.uscs.edu). To increase the size of the FISH signal for assessment of archival specimens, a probe pool was developed for each locus, comprising three overlapping BAC clones; a primary clone containing the gene of interest and at least one overlapping BAC clone on either side. This approach resulted in probe contigs for each locus, with DNA sequence extending the final probe size to approximately 500 kb. A summary of the BAC clones used is shown in SOM Table 1. To verify that each BAC pool had a unique cytogenetic location in healthy cells, all were first hybridized to metaphase preparations from six clinically healthy dogs, generated by conventional mitogen stimulation of peripheral lymphocytes (Breen et al. 1999). Single locus probe (SLP) multicolor FISH analysis was performed as described previously (Breen et al. 2004).

To establish a baseline of expected mean copy number of each probe when hybridized to non-neoplastic FFPE samples, each of the ten probes was first enumerated in nuclei of a series of 5 μm sections of FFPE specimens of healthy tissue matched controls. A minimum of 50 cells was imaged using a BioView Legato system (BioView, Israel) configured to acquire multiplane images of 19 adjacent focal planes at 0.5 μm increments. The mean copy number of each probe in >50 nuclei of 5 μm sections of FFPE biopsy specimens was then obtained using the same process and normalized to the mean of the corresponding controls. Classification of FISH signals as gains or losses was performed as described previously for human diagnostics (Gaiser et al. 2010) where the mean must be based on no fewer than 50 separate cells and aberrant signals must be found in at least 50 % of the cell population analyzed.

Comparative genomic hybridization

Oligo array CGH (oaCGH) was performed by co-hybridization of tumor (test) DNA and a common reference DNA sample, where the latter comprised an equimolar pool of genomic DNA samples from multiple healthy individuals of various breeds. DNA extracted from FFPE samples was slightly degraded, as expected, but this was shown to have no adverse effect on data quality. DNA was labeled using an Agilent SureTag Labeling Kit (Agilent Technologies, Santa Clara, CA) with all test samples labeled with Cyanine-3-dCTP and the common reference sample labeled with Cyanine-5-dCTP. Fluorochrome incorporation and final probe concentrations were determined using routine spectrophotometric parameters with readings taken from a Nanodrop1000. Fluorescently labeled test and reference samples were co-hybridized to Canine G3 180,000 feature CGH arrays (Agilent, AMADID 025522) for 40 h at 65 °C and 20 rpm, as described previously (Angstadt et al. 2011; Thomas et al. 2014). Arrays were scanned at 3 μm using a high-resolution microarray scanner (Agilent,

Model G2505C) and data extracted using Feature Extraction (v10.9) software. Scan data were assessed for quality by the 'Quality Metrics' report in

Agilent's Feature extraction software (v10.5) (Agilent Technologies)

Copy number data were analyzed with NEXUS Copy Number v7.0 software (Biodiscovery Inc., CA, USA). Copy number aberrations (CNAs) were identified using a FASST2 segmentation algorithm with a significance threshold of 5.5×10^{-6}. Aberrations were defined as a minimum of three consecutive probes with log2 tumor: reference value of >1.14 (high gain), 1.13 to 0.2 (gain), −0.23 to −1.1 (loss), <−1.1 (big loss). Recurrent CNAs within each subtype were determined within NEXUS using an involvement threshold of 50 %. Significance of these regions was then determined in NEXUS using the GISTIC algorithm (to identify regions with a statistically high frequency of copy number aberrations over background) with a G-score cut off of G>1.0 and a significance of Q<0.05. Copy number aberration frequency comparisons amongst sample groups were performed in NEXUS using Fisher's exact test with differential threshold of >50 % and significance $p<0.05$. Significance of each probe between the two groups was calculated in NEXUS using a Mann–Whitney test for median comparison.

Humanization of canine CGH data

Canine oaCGH data were recoded into 'virtual' human genome format to facilitate direct visual comparison of cytogenetic profiles of human and canine melanoma, as described previously (Thomas et al. 2011). Briefly, the genome coordinates of each of the 180,000 60-mer canine oligonucelotides were imported into the Liftover Batch Coordinate Conversion Tool (http://genome.ucsc.edu/cgi-bin/hgLiftOver), using default settings to establish the orthologous nucleotide sequence coordinates within the human genome sequence assembly (February 2009, GRCh37/hg19). Using these recoded coordinates, the tumor:reference signal intensity data for each array were reprocessed to output the oaCGH profile according to these 'virtual' human chromosome locations.

Clustering of oaCGH profiles

Hierarchical clustering was performed to evaluate how genome-wide CGH profiles differentiate between malignant and benign lesions. Hierarchical clustering using Ward's method for linkage was performed on the genome-wide log2 ratio data for each sample. Analysis was performed using the R statistical software, version 2.13.0 (R Development Core Team, Vienna, Austria) using the gplots package.

Statistical analysis of oaCGH and histology profiles

Correlation analysis was performed between oaCGH clusters and the corresponding histological characteristics to determine if DNA CNAs were significantly associated with pathological cellular morphologies. Initial analysis was based on pathological diagnosis alone. To test molecular association, two clusters were established based on oaCGH copy number profiles as performed above. These two groups were then assessed for statistical differences between histological characteristics. A Wilcoxon rank sum test was performed

for pigmentation and log mitotic values, and a Fisher's exact test was performed for association analysis with group status and nuclear atypia.

Results

Clinical assessment

A total of 49 canine melanomas and 18 benign melanocytomas were profiled by oaCGH during this study. Melanomas presented from two locations: the oral cavity (n=44) and unspecified haired skin (n=5). Benign melanocytomas presented primarily from haired skin (n=13) with rare presentation from the oral cavity (n=5). Breed was not a consideration in case selection, and there were 29 breeds of dog included in this study, with the most frequent being dogs of mixed breed (n= 14), accounting for 21 % of cases. In general, melanomas presented with a more aggressive histologic presentation including a significantly higher mitotic index (p= 2.98E-06), lower percent pigmentation (p=0.0002) and higher percent nuclear atypia (p=3.69E-10). A detailed summary of the histopathologic findings of each case is presented in Table 1.

Detection of CNA by oaCGH

Individuals represented within the oral (mucosal) melanoma cohort presented with complex genome-wide oaCGH profiles, with numerous recurrent changes resulting in a complex penetrance plot (Fig. 1). In most cases, the amplitude of each aberration (data not shown) was modest, suggesting either a unidirectional gain or loss of one copy of a locus within the majority of cells of the tumor, or a high level of cellular heterogeneity within the tumor cell population. This was clarified by FISH analysis of copy number status within individual cells, which corroborated single copy aberrations (described below). Highly recurrent CNAs (>50 % penetrance across the cohort) were assessed in detail (Table 2), several of which were statistically significant between subtypes using the GISTIC algorithm (SOM Table 2). For the cohort of oral melanomas, the most frequent DNA copy number gain was a 600 kb region of dog chromosome (CFA) 30 located at CFA30:19,102,383–19,660,901 (q=4.25E-10), along with whole chromosome gains of CFA 13, 17, 20, 29, and 36 Table 3. The most frequent DNA copy number losses involved the full lengths of CFA 22 and 27, as well as 15 and 122.5 kb segments located at CFA10:20,583,579–20,598,892 (q= 6.26E-05) and CFA26:30,241,704–30,306,343 (q= 1.34E-08), respectively. All genome coordinates are from canfam2.

Several regions of the genome had oaCGH profiles suggestive of structural changes, denoted by a copy number gain followed immediately by a loss, most notably on CFA 10 and CFA 30, both of which were found to be statistically significant using the GISTIC algorithm (SOM Table 2). The chromosome break point region on CFA 30, evident in 60 % of the oral melanomas analyzed, spans 5 Mb of sequence located between 14 and 19 Mb (Fig. 2). The log2 values within this region of CFA 30 were suggestive of a heterozygous loss followed by an immediate gain, with 97 % of affected cases suggestive of a copy number of ≥4.

Cutaneous melanomas, although small in number (n=5), also presented with recurrent CNAs (Fig. 1). The largest and most common aberration was a gain of CFA 20 that spanned 46.2

Mb of the chromosome CFA20:10,929,869–57,175,686, present in four of the five cases. The most frequent copy number losses included a 131 kb region of CFA6:48,260,040–49,569,575, a 385 kb region of CFA18:21,439,849–21,824,376, and the full length of chromosome 22. Due to the small number of cases, none of these aberrations were statistically significant using the GISTIC algorithm (SOM Table 2).

While individuals represented within the benign/ cutaneous melanocytoma cohort (n=18) presented with relatively stable oaCGH profiles, some recurrent aberrations were evident (Fig. 1). The most common aberration was gain of a 87 kb region of CFA27 CFA27:9,965,501–10,052,495 (q=3.40E-13). Other common aberrations were gains on CFA9:20,973,038–21,556,711 (q = 4.89E-09), CFA10:48,818,794–48,878,597 (q=3.95E-05), and CFA11:55,214,228–55,245,594 (q=4.99E-08). Melanocytomas had one significant recurrent copy number loss, a 200 kb region at CFA8:76,368,492–76,582,392 (q=7.78E-04).

Comparison of melanomas to melanocytomas

A number of CNAs were either detected in one subtype only or shared between just two of the three subtypes (SOM Table 3). Cutaneous melanomas and melanocytomas shared several common recurrent aberrations, which were either rare or absent in oral melanomas, most significantly a 17.5 Mb region of gain at CFA20:39,655,694–57,175,686, detected in approximately 45 % (8/18) of melanocytomas and 80 % (4/5) of cutaneous melanomas (in CM q<0.01). Another notable similarity between these two groups was the presence of a 9 Mb copy number gain between 35 and 44 Mb on chromosome 30 (Fig. 2a, c). There were no aberrations shared between cutaneous and oral melanomas at the 50 % differential level. However, when the stringency was dropped to 40 %, several shared regions became evident, including a 140 kb loss of CFA3:65,280,294–65,432,693 and a 260 kb gain of CFA13:8,127,632–8,394,801 (data not shown). Aberrations unique to one subtype were also evident. Deletion of a 385 kb segment of CFA18 at CFA18:21,439,849–21,824,376 was highly recurrent only in cutaneous melanomas and a complex copy number profile along a 13 Mb region of CFA30 CFA30:8,290,472–21,411,530 was observed only in oral melanomas.

Hierarchical clustering of all melanocytic lesions

Hierarchical clustering of segmented oaCGH profiles separated the 67 samples into three well-defined groups (Fig. 3). One of the groups contained only malignant samples, the second contained malignant samples with a single benign lesion, and the third group contained a mix of benign (n=17) and malignant samples (n=21). The clustering of 21 malignant samples with the benign samples is partially explained by the reduced level of aberrations within those particular malignant lesions.

Clusters were further evaluated by consideration of their histological characteristics, to identify correlation of cellular morphology with genome-wide CGH profiles. Malignant samples (n=21/44) that clustered with benign samples had significantly higher pigmentation (p=0.018), lower mitotic index (p=0.023), and a lower, but not statistically significant, nuclear atypia (p=0.222) than the group of malignant melanomas that clustered together

(n=28). These data demonstrate that molecular aberrations in canine malignant melanomas correlate with the cellular phenotype and histology, suggesting the potential utility of molecular markers to differentiate between histologically ambiguous lesions.

Detection of CNA by FISH analysis of FFPE sections

All targeted loci (n=10) evaluated by FISH analysis showed aberrant copy number in oral melanomas. The most frequent unidirectional changes were a gain of c-*MYC* (80 % of cases) and loss of *CDKN2A* (68 % of cases) and *RB1* (35 % of cases). The other seven loci evaluated showed bidirectional changes (Fig. 4a). As expected, based on the whole genome oaCGH data, the extent of SLP CNAs in the benign lesions was lower (Fig. 4b). The most common of the targeted CNAs evident in the benign lesions were loss of *TP53* and *CDKN2A*. It is important to note that these aberrations were observed only as a heterozygous loss, indicating the retention of one allele for production of downstream product (if unmutated). Interestingly, neither tumor types showed a significant copy number amplification of regions encompassing *BRAF* or *CCND1*, both of which are highly aberrant in human UV-induced cutaneous melanomas. The population of canine oral melanomas showed a combination of both copy number gain and loss for these gene regions, suggesting overall chromosome instability, but not targeted gene amplification.

Comparison of canine to human melanocytic lesions

Humanization of the canine oaCGH data allowed for direct comparison of the canine data collected in this study to the CNA status of human melanomas accessible from the previous studies. When aligned with genome wide oaCGH profiles of different subtypes of human melanoma, striking similarities were present between canine oral melanoma and both human mucosal melanoma and human acral melanoma (Fig. 5). Human mucosal and acral melanomas have been shown to present with more complex genome-wide oaCGH profiles than cutaneous melanomas (Curtin et al. 2005; Furney et al. 2012; Thomas et al. 2014), paralleling the data for canine melanomas in the current study. Many CNAs were shared between human and dog, including a characteristic complex oaCGH profile involving the evolutionarily conserved chromosome segments represented by human chromosome chr15:38,701,609–49,824,200 and canine chromosome CFA30:8,290,472–21,411,530. Notably, this distinct aberration was not detected in canine cutaneous melanomas or in human common cutaneous melanomas. Human mucosal and acral melanomas showed additional smaller shared aberrations (Table 4).

Discussion

Aberrations within melanomas and melanocytomas: Implications for tumorigenenesis

As with human melanomas, canine melanomas present with cytogenetically distinct profiles based on malignancy and the anatomic location in which they arise. The most striking evidence for this is the presence of a characteristic aberration of CFA 30 in oral melanomas, which is absent in cutaneous lesions. Melanocytomas, which are primarily cutaneous, had noticeably fewer aberrations than both subtypes of melanoma. However, approximately 40 % of these were shared with cutaneous melanoma, including the recurrent copy number gain of CFA20:39,655,694–57,175,686, evident in cutaneous but not oral lesions (SOM

Table 2). These features may represent aberrations necessary for the growth of canine melanocytic tumors from the cutaneous epithelium and subsequent targeted investigation into this genomic region may elucidate tumor initiation specific to this tissue location. Along with significant potential for the future use of molecular differentiation as part of the diagnostic process, the recognition of molecular profiles provides insight into the initiation and development of the different subtypes of melanomas. Ultimately, this knowledge may lead to the development of specific treatment regimes based on the site of primary tumor growth.

The most recurrent aberration specific to the oral melanoma cohort was a distinctive complex copy number profile on CFA 30, present in 60 % of cases and characteristic of a structural chromosomal rearrangement. Due to the high incidence of this particular complex CNA, it is probable the rearrangement is significant for the development of canine oral melanoma or progression towards a malignant phenotype. This aberration may be of potential for use as a signature to differentiate between lesions that are likely to progress, requiring additional treatments, and those that are likely to remain benign; however, additional studies correlating the presence of this pattern to clinical outcome are needed. Further study into the cause and biological effect of the breakage may also reveal why oral melanomas are behaviorally more aggressive than other melanocytic subtypes. The 5 Mb region of genome sequence surrounding the breakage (CFA30:15–20 Mb) is within a gene desert, flanked by gene-rich areas. This is also a feature of unstable chromosome regions in the human genome, such as the breakpoint cluster region (*BCR*) at 22q11.23.

Within the complex region of CNA on CFA 30 are nine annotated genes, six of which increased in copy number while three decreased in copy number (Table 3). One gene with a copy number loss, *SPRED1*, is a known suppressor of Ras/MAP-K activation. Since deletion of *SPRED1* can positively regulate the activation of the RAS/MAP-K pathway, this aberration in canine melanoma suggests a possible mechanism of tumorigenesis. The involvement of the MAP-K pathway is also supported by the presence of *TRPM7* within the region of copy number gain on CFA 30. Increase in gene dosage may be associated with increased expression, and over-expression of *TRPM7* has been shown to be involved in both melanoma development (Guo et al. 2012) and the regulation of the MAP-K pathway (Meng et al. 2013). Additionally, targeted FISH analysis of canine oral melanomas indicated copy number gain of both *C-KIT*, which initiates the RAS/MAP-K pathway, and *C-MYC*, which is downstream of the MAP-K phosphorylation cascade. Both *C-MYC* and *C-KIT* showed copy number gain in canine oral melanomas (80 and 65 % of cases, respectively), further supporting the involvement of the MAP-kinase signaling pathway in the development of canine oral melanomas. Previous studies have shown the activation of the MAP-K signaling cascade, but were unable to fully elucidate the mechanism (Angstadt et al. 2012; Fowles et al. 2013). Copy number gain, and subsequent overexpression, of *TRPM7* and loss of *SPRED1* may represent such a mechanism.

Aberrations detected in both malignant forms of canine melanoma, but not in melanocytomas, suggest that these specific mutations are associated with the development of these malignant and aggressive neoplasms. This was further confirmed by the high degree of correlation between patterns of genome-wide CNAs and cellular histology. Malignant

melanomas presenting with less complex oaCGH profiles (similar to those of benign lesions) had noticeably different cellular morphologies from those with complex copy number profiles. This supports the underlying molecular basis of cellular phenotype and implies that specific CNAs present within these particular malignant lesions give rise to a more malignant phenotype. Regions of shared CNA within the malignant populations contain numerous genes (Table 3). In light of the cellular function of the gene product, the evaluation of dysregulation of these genes may in turn contribute to understanding of malignant characteristics, including complex genome-wide CNAs, dedifferentiated cell morphologies, and presentation of histologically ambiguous features. For example, the most frequent aberration observed in both cutaneous and oral melanomas was a copy number loss of the segment CFA3:62,368,641–62,381,281. Within this region is the coding sequence for *TACC3*, which acts as a stabilizer of mitotic spindles during mitosis and has been proposed to play a role in cell differentiation.

All ten loci evaluated by FISH analysis showed aberrant copy number in canine oral melanomas. Seven of the loci evaluated showed a combination of gains and losses, suggesting that the genomic instability at these regions was more random than targeting functional pathway alterations. This suggestion is supported by the fact that no homozygous losses and few high amplification events were detected involving any of these seven loci. Three genes showed only unidirectional CNA among the cohort, *C-MYC*, *RB1*, and *CDKN2A*, suggesting these are not merely random CNAs due to end-stage mitotic instability, but rather targeted alterations advantageous to tumor development. The dysregulation of mRNA expression in these genes has been previously established (Ritt et al. 1998; Koenig et al. 2002; Bianco et al. 2003). The identification of the presence of these CNAs now offers a mechanism by which tumor cells regulate gene expression leading to tumorigenesis of canine oral melanoma.

Comparison of canine copy number changes to human melanocytic lesions

Oral mucosal melanomas in humans are rare and poorly understood, representing only 2 % of all melanomas (Chang et al. 1998). Due to the small number of cases, limited large-scale genomic research has been performed and so details of the genetics of development of mucosal melanomas and the majority of genetic drivers remain unknown. Through clinical observations of similar anatomical location and behavior, it has been proposed that the mucosal subtype of human melanoma would be analogous to oral canine melanomas, which would support their use as a model system to study the development of these rare tumors. Curtain and colleagues first assembled cytogenetic hallmarks of human acral and mucosal melanoma through BAC-array CGH in 2005 (Curtin et al. 2005). Using those published data as a reference, we were able to directly compare CNAs reported in these forms of human melanoma with those identified in canine cases in the present study. The comparison revealed mucosal melanomas in both species to have a complex genome-wide copy number profile. This is suggestive of decreased genome stability and increased susceptibility to karyotype rearrangements, corroborated by recent whole-genome sequence data (Furney et al. 2012; Thomas et al. 2014). In general, the CNAs most common to canine melanoma were shared with those detected in human mucosal melanomas. Moreover, the canine CNAs were different from those evident in UV-induced human cutaneous melanomas, which also differ

from human mucosal melanomas. The most remarkable similarity between canine melanomas and their human ortholog was a conserved and complex copy number profile along the length of CFA 30/HSA 15. The characteristic copy number signature on HSA15 has been reported only in mucosal and acral melanomas. We propose that this characteristic feature is associated with a key evolutionarily conserved mechanism of pathogenesis in the development and/or progression of mucosal melanomas. It was also noted that no individual within the canine cohort showed the characteristic *BRAF* amplification or associated *CCND1* amplification commonly detected in UV-induced cutaneous melanomas in humans. Other notable conserved mutations are seen as a gain on CFA 13 (cf HSA chr4:70,508,745–70,808,489), loss of CFA 4 and 11 (cf HSA chr5:50,515,301–76,556,132), and gain of CFA 10 and 26 (cf HSA chr12:48,133,151–52,785,962). These imply that the underlying pathway of development in all mucosal melanomas, regardless of species, may be different to that of cutaneous UV-induced melanomas. They also underpin more detailed and statistically powerful studies of the etiology and treatment of mucosal melanomas.

Previous comparative studies of melanoma have primarily relied solely on histology and targeted sequencing, highlighting the dissimilarity of canine melanoma and human common cutaneous melanoma, and limited homology with mucosal melanomas. In agreement with other recent proposals (Fowles et al. 2013; Gillard et al. 2014; Simpson et al. 2014), this study now bolsters the burgeoning role of the dog model in investigations of pathogenesis of non-UV induced mucosal melanomas. The genome-wide molecular cytogenetic analysis in this study revealed remarkable similarities shared between human and dog mucosal melanomas. Pathways specific to melanogenesis of mucosal surfaces may be elucidated by a comparative oncology approach, with integrated the consideration of -omics data from both species.

Supplementary Material

Refer to Web version on PubMed Central for supplementary material.

Acknowledgments

This study was funded in part by a clinical trial award from Antech Diagnostics (awarded to MB) and with funds from the NCSU Cancer Genomics Fund (MB). KP was supported in part by funds from a Comparative Biomedical Sciences Graduate Studentship, and in part by a Department of Education GAANN Fellowship. We thank Rachael Thomas for assistance in humanizing the canine CGH data and Christina Williams for sample coordination. SR was supported by T32GM081057 from the National Institute of General Medical Sciences and the National Institute of Health.

Abbreviations

BAC	Bacterial artificial chromosome
BRAF	V-raf murine sarcoma viral oncogene homolog B1
C-KIT	V-kit Hardy-Zuckerman 4 feline sarcoma viral oncogene homolog
C-MYC	V-myc myelocytomatosis viral oncogene homolog (avian)
CCND1	G1/S-specific cyclin-D1

CDK4	Cyclin-dependent kinase 4
CDKN1A	Cyclin-dependent kinase inhibitor 1A
CDKN2A	Cyclin-dependent kinase inhibitor 2A
CFA	*Canis familiaris* (also used as a prefix to chromosome numbers)
CNA	Copy number aberration
FFPE	Formalin-fixed paraffin-embedded
FISH	Fluorescence in situ hybridization
H&E	Hematoxylin and eosin
HSA	*Homo sapiens* (also used as a prefix to chromosome numbers)
MAP-K	Mitogen-activated protein kinases
oaCGH	Oligo-array comparative genomic hybridization
PTEN	Phosphatase and tensin homolog
RAS	Rat sarcoma gene
RB-1	Retinoblastoma 1
SLP	Single locus probe
SPRED1	Sprouty-related, EVH1 domain containing 1
TACC3	Transforming, acidic coiled-coil containing protein 3
TP53	Cellular tumor antigen p53
TRPM7	Transient receptor potential cation channel, subfamily M, member 7

References

Angstadt AY, Motsinger-Reif A, Thomas R, et al. Characterization of canine osteosarcoma by array comparative genomic hybridization and RT-qPCR: Signatures of genomic imbalance in canine osteosarcoma parallel the human counterpart. Genes Chromosom Cancer. 2011; 50(11):859–874. [PubMed: 21837709]

Angstadt AY, Thayanithy V, Subramanian S, Modiano JF, Breen M. A genome-wide approach to comparative oncology: High-resolution oligonucleotide aCGH of canine and human osteosarcoma pinpoints shared microaberrations. Cancer Genet. 2012; 205(11):572–587. [PubMed: 23137772]

Bastian BC, Olshen AB, LeBoit PE, Pinkel D. Classifying melanocytic tumors based on DNA copy number changes. Am J Pathol. 2003; 163(5):1765–1770. [PubMed: 14578177]

Bauer J, Bastian BC. Distinguishing melanocytic nevi from melanoma by DNA copy number changes: Comparative genomic hybridization as a research and diagnostic tool. Dermatol Ther. 2006; 19:40–49. [PubMed: 16405569]

Bergman P. Canine oral melanoma. Clin Tech Small Animal Pract. 2007; 22(2):55–60.

Bianco SR, Sun J, Fosmire SP, et al. Enhancing antimelanoma immune responses through apoptosis. Cancer Gene Ther. 2003; 10(9):726–736. [PubMed: 12944992]

Blokx WAM, van Dijk MCRF, Ruiter DJ. Molecular cytogenetics of cutaneous melanocytic lesions diagnostic, prognostic and therapeutic aspects. Histopathology. 2010; 56(1):121–132. [PubMed: 20055910]

Breen M. Update on genomics in veterinary oncology. Top Companion Animal Med. 2009; 24(3):113–121.

Breen M, Bullerdiek J, Langford CF. The DAPI banded karyotype of the domestic dog (Canis familiaris) generated using chromosome-specific paint probes. Chromosom Res. 1999; 7(7):575.

Breen M, Hitte C, Lorentzen TD, et al. An integrated 4249 marker FISH/RH map of the canine genome. BMC Genomics. 2004; 5(1):65. [PubMed: 15363096]

Chang AE, Karnell LH, Menck HR. The national cancer data base report on cutaneous and noncutaneous melanoma. Cancer. 1998; 83(8):1664–1678. [PubMed: 9781962]

Curtin JA, Fridlyand J, Kageshita T, et al. Distinct sets of genetic alterations in Melanoma New England. J Med. 2005; 353(20):2135–2147.

Fowles J, Denton C, Gustafson D. Comparative analysis of MAPK and PI3K/AKT pathway activation and inhibition in human and canine melanoma. Veterinary Comparative Oncology. 2013 Epub ahead of print.

Furney SJ, Turajlic S, Fenwick K, et al. Genomic characterisation of acral melanoma cell lines. pigment cell & melanoma research: no-no. 2012

Furney SJ, Turajlic S, Stamp G, et al. Genome sequencing of mucosal melanomas reveals that they are driven by distinct mechanisms from cutaneous melanoma. J Pathol. 2013; 230(3):261–269. [PubMed: 23620124]

Gaiser T, Kutzner H, Palmedo G, et al. Classifying ambiguous melanocytic lesions with FISH and correlation with clinical long-term follow up. Mod Pathol. 2010; 23(3):413–419. [PubMed: 20081813]

Gillard M, Cadieu E, De Brito C, et al. Naturally occurring melanomas in dogs as models for non-UV pathways of human melanomas. Pigment Cell Melanoma Res. 2014; 27(1):90. [PubMed: 24112648]

Guo H, Carlson JA, Slominski A. Role of TRPM in melanocytes and melanoma. Exp Dermatol. 2012; 21(9):650–654. [PubMed: 22897572]

Koenig A, Bianco SR, Fosmire S, Wojcieszyn J, Modiano JF. Expression and significance of p53, Rb, p21/waf-1, p16/ink-4a, and PTEN tumor suppressors in canine melanoma. Vet Pathol. 2002; 39(4): 458–472. [PubMed: 12126149]

Kudnig ST, Ehrhart N, Withrow SJ. Survival analysis of oral melanomas in dogs. Vet Cancer Soc Proc. 2003; 23(39)

Meng X, Cai C, Wu J, et al. TRPM7 mediates breast cancer cell migration and invasion through the MAPK pathway. Cancer Lett. 2013; 333(1):96–102. [PubMed: 23353055]

Newman SJ, Jankovsky JM, Rohrbach BW, LeBlanc AK. C-kit expression in canine mucosal melanomas. Vet Pathol. 2011; 49(5):760–765. [PubMed: 21825314]

Overly B, Goldschmidt MH, Schofer F. Canine oral melanoma: a retrospective study. veterinary cancer society proceedings. 2001; 21(43)

Ramos-Vara JA, Beissenherz ME, Miller MA, et al. Retrospective study of 338 canine oral melanomas with clinical, histologic, and immunohistochemical review of 129 cases. Vet Pathol. 2000; 37(6): 597–608. [PubMed: 11105949]

Ritt MG, Wojcieszyn J, Modiano JF. Functional loss of p21/Waf-1 in a case of benign canine multicentric melanoma. Vet Pathol. 1998; 35(2):94–101. [PubMed: 9539362]

Simpson RM, Bastian BC, Michael HT, et al. Sporadic naturally occurring melanoma in dogs as a preclinical model for human melanoma. Pigment Cell Melanoma Res. 2014; 27(1):37–47. [PubMed: 24128326]

Smedley RC, Spangler WL, Esplin DG, et al. Prognostic markers for canine melanocytic neoplasms: a comparative review of the literature and goals for future investigation. Vet Pathol. 2011; 48(1):54–72. [PubMed: 21266721]

Smith SH, Goldschmidt MH, McManus PM. A comparative review of melanocytic neoplasms. Vet Pathol. 2002; 39(6):651–678. [PubMed: 12450197]

Spangler WL, Kass PH. The histologic and epidemiologic bases for prognostic considerations in canine melanocytic neoplasia. Vet Pathol. 2006; 43(2):136–149. [PubMed: 16537931]

Thomas R, Seiser EL, Motsinger-Reif A, et al. Refining tumor-associated aneuploidy through 'genomic recoding' of recurrent DNA copy number aberrations in 150 canine non-Hodgkin lymphomas. Leuk Lymphoma. 2011; 52(7):1321–1335. [PubMed: 21375435]

Thomas R, Borst L, Rotroff D, et al. Genomic profiling reveals extensive heterogeneity in somatic DNA copy number aberrations of canine hemangiosarcoma. Chromosom Res. 2014; 22:305–319.

Villamil JA, Henry CJ, Bryan JN, et al. Identification of the most common cutaneous neoplasms in dogs and evaluation of breed and age distributions for selected neoplasm. JAVMA. 2011; 239(7): 960–965. [PubMed: 21961635]

Withrow, SJ., Vail, DM., Page, R. Small animal clinical oncology. Elsevier; 2013.

Xie T, Lamb GDA Jr. A comprehensive characterization of genome-wide copy number aberrations in colorectal cancer reveals novel oncogenes and patterns of alterations. PLoS One. 2012; 7(7):e42001. [PubMed: 22860045]

Xie T, D' Ario G, Lamb JR, Martin E, Wang K, Tejpar S, Delorenzi M, Bosman FT, Roth AD, Yan P, Bougel S, Di Narzo AF, Popovici V, Budinská E, Mao M, Weinrich SL, Rejto PA, Hodgson JG. A comprehensive characterization of genome-wide copy number aberrations in colorectal cancer reveals novel oncogenes and patterns of alterations. 2012; doi: 10.1371/journal.pone.0042001

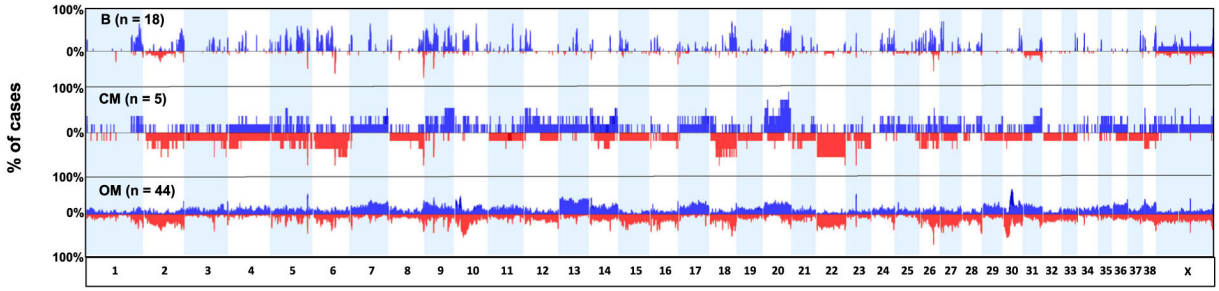

Fig. 1.

aCGH analysis of primary canine oral melanoma (*OM*), primary canine cutaneous melanoma (*CM*), and canine cutaneous melanocytoma (*B*). Penetrance plots of recurrent CNAs, at 26 kb intervals, identified within 67 canine melanocytic lesions. Genomic locations are plotted along the *x*-axis, and the *y*-axis indicates the percentage of the three subtypes with copy number gain (shown in *blue* above the midline) or loss (shown in *red* below the midline) of the corresponding intervals along each chromosome. In oral melanomas (OM, n=44), the most frequent gain was located on CFA30:18,527,413–18,592,465, along with whole chromosome gains of CFA 13, 17, 20, 29, and 36. The most frequent losses were found on CFA10:20,583,579–20,598, 892, CFA26:30,241,704–30,306,343, CFA30:10,620,776–10,658,526, and all of CFA 2, 22, and 27. In cutaneous melanomas (CM, n=5), the largest and most common aberration was a gain of CFA20:10,929,869–57,175,686. In melanocytomas (B, n=18), the most frequent aberration was a gain of a small region of CFA27:9,965,501–10,052,495, as well as less frequent gains on CFA9:20,973,038–21,556,711, CFA10:48,818,794–48,878,597, and CFA11:55,214,228–55,245,594

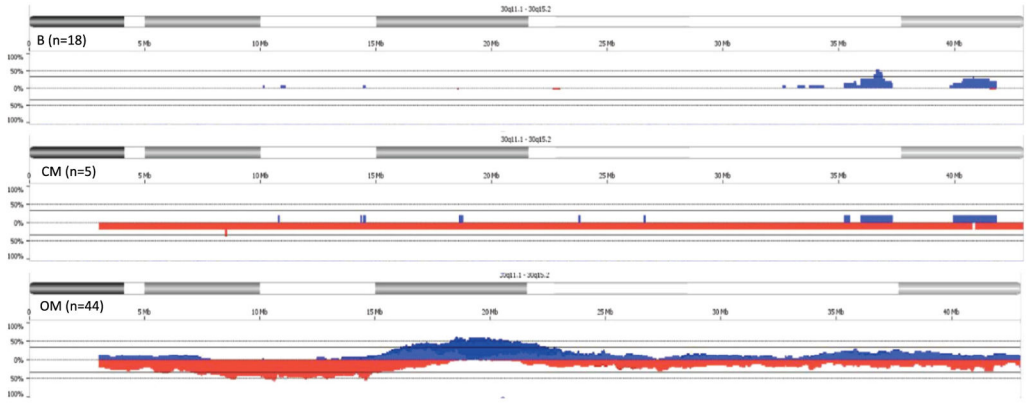

Fig. 2.

Penetrance plots of DNA copy number aberrations along the length of CFA 30 in oral melanomas (*OM*), cutaneous melanomas (*CM*), and melanocytomas (*B*). Oral melanomas showed a distinct pattern of copy number loss (spanning 3–18 Mb) partially overlapping a region of copy number gain (spanning 12–25 Mb), indicative of a variable chromosome breakage event. This breakage region, centered at 15–18 Mb was not present in either cutaneous melanomas or benign melanocytomas. Fifty percent (n=9/18) of melanocytomas showed a gain of two small regions at the distal end of CFA 30 (35–37 and 40–42 Mb), also seen in 20 % (n=1/5) of cutaneous melanomas

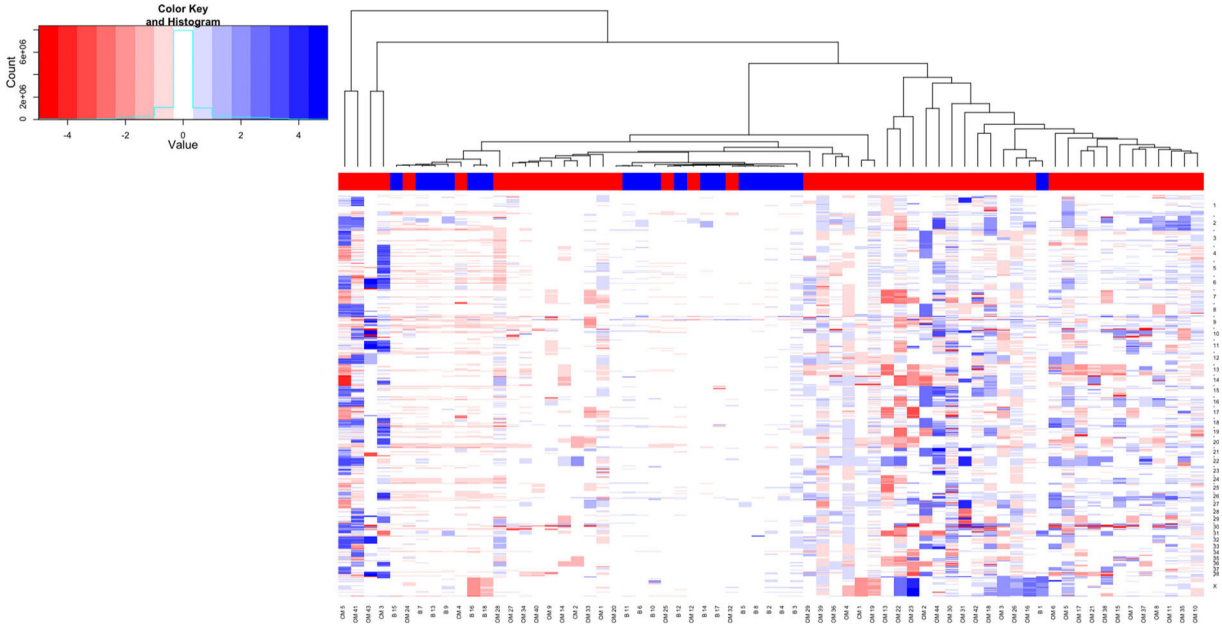

Fig. 3.

Clustering analysis of oaCGH derived genome wide DNA copy number data of 44 primary canine oral melanomas, five primary canine cutaneous melanomas, and 18 primary canine melanocytomas. Segmented oaCGH profiles were subjected to hierarchical clustering. Individual cases are plotted along the *x*-axis, with chromosomes plotted along the *y*-axis. Cases were grouped and a linage tree of relatedness schematic is drawn above. *Blue*, *red*, *and white* represent copy number gain, loss, and neutrality. The log2 ratio is represented in the intensity of the coloration gradient as per the inset. *Colored bars* above each sample indicate malignant (*red*) or benign (*blue*) cases. In general, cases with more complex copy number profiles clustered together. There were 21 malignant melanomas, each with few copy number aberrations, which clustered into the same bin as all but one of the benign lesions. Further analysis revealed that these 21 cases had histological characteristics significantly different from the subset of 23 malignant melanomas that clustered together and separately. The one benign lesion that clustered with a group of malignant lesions had just two whole chromosome gains, CFA 31 and X

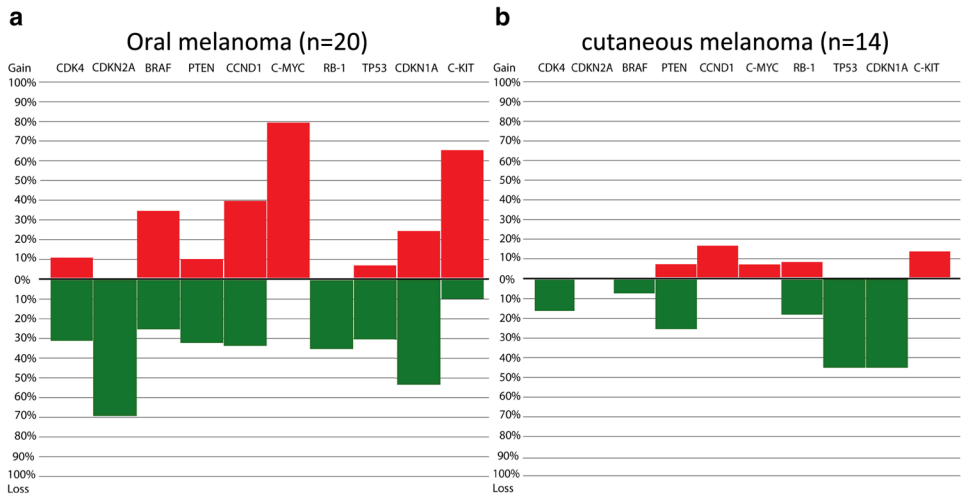

Fig. 4.

SLP FISH derived copy number status of ten targeted loci in **a** primary canine oral melanoma and **b** canine melanocytoma. Percentage of cases with gains/losses is plotted above/below the *y*-axis. Full locus identity and location are provided in SOM Table 1. Canine oral melanomas showed higher percentage of cases with targeted genomic aberrations than benign melanocytomas, validating the oaCGH data. It also revealed targeted regions with unidirectional changes, suggesting their involvement in downstream pathway dysregulation and tumorigenesis

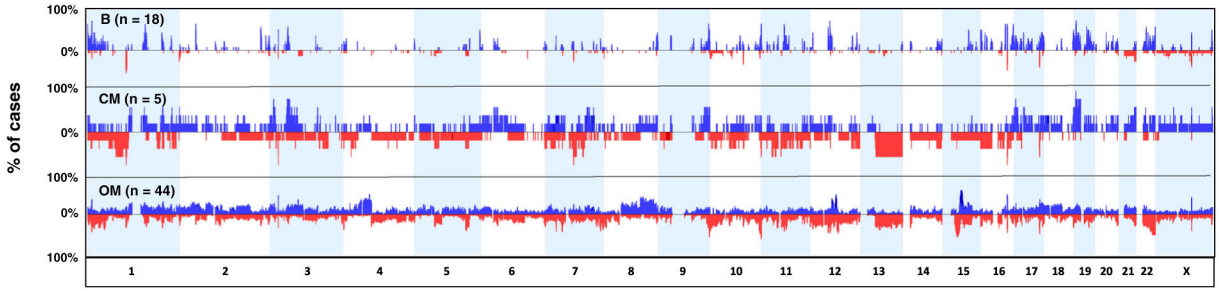

Fig. 5.

Canine oral melanoma (*OM*), cutaneous melanoma (*CM*), and benign melanocytoma (*B*) oaCGH profile data recoded as human. Canine oral melanomas (n=44), cutaneous melanomas (n=5), and cutaneous melanoctyomas (n=18) were recoded and output with human genome coordinates. This allowed for comparison to known aCGH profiles compiled for human melanoma subtypes. Hallmarks of human mucosal melanoma are copy number amplification of HSA 1q31, 4q12, 12q14, 11q13, 8q, and 6p as well as copy number loss of 3q, 4q, 8p, 10, 11p, and 21q (Curtin et al. 2005). Similar aberrations were found within the canine oral melanoma population. Most notably, the breakage area on CFA 30 matches a similar pattern of loss followed by gain seen on HSA 15, the orthologous region on the human genome

Table 1

Histological description of primary tumors from formalin-fixed paraffin embedded (FFPE) and fresh frozen samples

Cases	Primary site	Breed	Age (year)	Sex	Mitotic index	Pigmentation (%)	Nuc. atypia	Junctional activity	Tissue subtype
FFPE oral melanomas									
OM 1	Oral–mandible w/g&t	Golden retriever	11	F	41	<5	High	Yes	Mixed
OM 2	Oral–caudal oral cavity	English shepherd dog	9	M	13	<5	High	Yes	Polygonal
OM 3	Oral–gum	Airedale terrier	11	F	8	40	Low	No	Mixed
OM 4	Oral–maxilla	Scottish terrier	10	F	39	0	High	No	Spindeloid
OM 5	Oral	Golden retriever	9	F	48	10	High	No junction available	Spindeloid
OM 6	Oral	Mixed	10	M	50	5	High	No	Polygonal
OM 7	Oral	Schipperke	14	M	44	0	Med	No junction available	Spindeloid
OM 8	Oral	Rottweiler	6	M	34	50	High	No junction available	Polygonal
OM 9	Oral	Beagle	12	F	4	50	High	Yes	Polygonal
OM 10	Oral	Cocker spaniel	n/a	M	140	0	High	Yes	Polygonal
OM 11	Oral	Not identified	16	M	8	0	High	No	Spindeloid
OM 12	Oral	Australian shepherd	8	M	2	50	Low	Yes	Mixed
OM 13	Oral	Labrador retriever	10	M	42	5	High	Yes	Polygonal
OM 14	Oral	Yorkshire terrier	11	F	26	50	Med	Yes	Polygonal
OM 15	Oral	Labrador retriever	9	M	48	0	Med	Yes	Polygonal
OM 16	Oral	Golden retriever	9	F	4	100	Low	No junction available	Spindeloid
OM 17	Oral	Mixed	13	M	170	0	High	No	Mixed
OM 18	Oral	Mixed	n/a	F	85	5	low	Mixed	Spindeloid
OM 19	Oral	Labrador retriever	13	M	3	10	High	Mixed	Ulcerated mix
OM 20	Oral - Lip	Jack russell terrier	10	F	11	5	Low	No junction available	Polygonal
OM 21	Oral	Not identified	15	F	34	0	Low	No junction available	Mixed
OM 22	Oral	Lhasa apso	15	F	9	<5	Low	Yes	Ulcerated polygonal
OM 23	Oral	Mixed	14	M	14	0	High	Yes	Mixed
OM 24	Oral	Labrador retriever	8	M	30	95	Low	Yes	Mixed
OM 25	Oral	Cocker spaniel	13	M	12	50	Low	No	Polygonal
OM 26	Oral	Mixed	10	F	5	20	High	Yes	Necrotic spindeloid
OM 27	Oral	English springer spaniel	n/a	F	6	0	High	No	Spindeloid

Cases	Primary site	Breed	Age (year)	Sex	Mitotic index	Pigmentation (%)	Nuc. atypia	Junctional activity	Tissue subtype
OM 28	Oral	Not identified	13	F	33	<5	Mid	No	Polygonal
OM 29	Oral	Pekinese	14	M	12	0	High	Yes	Polygonal
OM 30	Oral	Flat-coated retriever	10	M	50	0	High	No junction available	Mixed
OM 31	Oral	Gordon setter	11	M	18	5	High	No	Mixed
OM 32	Oral	Yorkshire terrier	9	M	7	10	Low	No	Spindeloid
Fresh oral melanomas									
OM 33	Oral	Mixed	n/a	M	67	>50	High	Yes	Mixed
OM 34	Oral	Mini schnauzer	n/a	F	0	>50	Low	No	Polygonal
OM 35	Oral	Belgian malamute	n/a	F	3	<5	High	No junction available	Spindeloid
OM 36	Oral	Mixed	n/a	M	15	>50	High	Yes	Mixed
OM 37	Oral	Poodle	n/a	M	19	<5	High	No junction available	Polygonal
OM 38	Oral	Mini schnauzer	10	F	26	70	Med	Yes	Spindeloid
OM 39	Oral	Labrador retriever	14	F	N/a	0	N/a	N/a	N/a
OM 40	Oral	Mixed	14	F	0	50	No	No junction available	Polygonal
OM 41	Oral	German shorthaired Pointer	10	F	5	50	High	No junction available	Polygonal
OM 42	Oral	Cocker spaniel	10	M	N/a	0	High	No junction available	Polygonal
OM 43	Oral	Poodle	12	F	40	0	Med	No junction available	Mixed
OM 44	Oral	English setter	11	F	15	0	High	Yes	Polygonal
FFPE melanocytomas									
B 1	Oral	Miniature schnauzer	7	M	0	80	No	No junction available	Too pigmented
B 2	Skin	Golden retriever	5	M	0	80	No	No junction available	Spindeloid
B 3	Skin	Not identified	8	F	0	25	No	No	Mixed
B 4	Skin	Poodle	10	F	2	50	Low	No	Polygonal
B 5	Skin	Boxer	13	M	2	2	Low	Mix	Mixed
B 6	Skin	Jack Russell Terrier	12	M	2	20	Low	No junction available	Spindeloid
B 7	Skin	Mixed	13	M	2	80	No	Yes	Polygonal
B 8	Skin	Miniature schnauzer	8	M	2	20	Low	No junction available	Spindeloid
B 9	Skin	Not identified	7	F	4	60	No	Yes	Spindeloid
B 10	Oral	Mixed	7	M	3	80	Low	Yes	Spindeloid
B 11	Skin	Lhasa apso	14	F	5	20	No	No	Spindeloid
B 12	Skin	Mixed	6	M	0	80	No	Yes	Spindeloid

Cases	Primary site	Breed	Age (year)	Sex	Mitotic index	Pigmentation (%)	Nuc. atypia	Junctional activity	Tissue subtype
B 13	Skin	Portuguese water dog	6	F	1	100	No	No junction available	Spindeloid
B 14	Skin	Pug	5	M	0	100	Low	No junction available	Spindeloid
B 15	Skin	Miniature schnauzer	8	M	1	90	No	Yes	Too pigmented
B 16	Oral	Mixed	10	M	0	90	Low	Yes	Too pigmented
B 17	Oral	Mixed	6	M	3	0	Low	No	Mixed
B 18	Oral	Gordon setter	11	M	5	50	High	No	Ulcerated
Cutaneous melanomas fresh and FFPE									
CM 1	Skin - ear tip	Doberman pincher	11	M	4	50	Low	Yes	Spindeloid
CM 2	Skin - foot pad	German shepherd	9	F	5	70	High	No junction available	Spindeloid
CM 3	Skin	Golden retriever	14	M	8	0	High	No junction available	Spindeloid
CM 4	Skin	Mixed	12	F	50	0	High	Yes	Spindeloid
CM 5	Skin	Basset hound	8	F	7	0	Low	Yes	Mixed

Table 2

Genome wide DNA copy number aberrations with at least 50% penetrance for three subtypes of canine melanocytic lesions, oral melanoma (OM), benign melanocytoma (B), and cutaneous melanoma (CM)

Region chr:bp start-bp end	Length (bp)	Cytoband	Event	Genes	Frequency (%)
OM *n*=44					
chr30:19,102,383–19,660,901	558,518	q14.1	CN gain	7	61.36
chr30:19,876,904–19,996,814	119,910	q14.1	CN gain	1	61.36
chr30:20,116,984–20,240,659	123,675	q14.1	CN gain	2	59.09
chr30:20,387,339–20,525,268	137,929	q14.1	CN gain	3	59.09
chr10:20,583,579–20,598,892	15,313	q21	CN loss	0	56.82
chr26:30,261,091–30,306,343	45,252	q24	CN loss	2	75.00
CM *n*=5					
chr20:10,929,869–57,175,686	46,245,817	q11–17	CN gain	359	80.00
chr18:21,439,849–21,824,376	384,527	q21	CN loss	1	80.00
chr23:23,552,949–23,718,671	165,722	q21.1	CN loss	0	80.00
chr6:48,260,040–49,569,575	1,309,535	q23.1	CN loss	0	80.00
chr22:63,472,754–63,531,977	59,223	q24	CN loss	2	80.00
chr5:81,157,085–81,422,820	265,735	q35	CN loss	0	80.00
BM *n*=18					
chr27:9,965,501–10,052,495	86,994	q12	CN gain	5	73.33
chr9:20,973,038–21,556,711	583,673	q14	CN gain	9	66.67
chr10:48,818,794–48,878,597	59,803	q21	CN gain	1	66.67
chr11:55,214,228–55,245,594	31,366	q21	CN gain	7	66.67
chrX:1-143,538	143,538	p22.3	CN gain	12	60.00
chr27:5,862,415–6,022,827	160,412	q11	CN gain	15	60.00
chr7:44,579,697–44,813,300	233,603	q17	CN gain	12	60.00
chr20:60,767,150–61,000,000	232,850	q17	CN gain	18	60.00
chr6:41,862,591–42,008,647	146,056	q22	CN gain	13	60.00
chr9:53,793,547–53,944,034	150,487	q25	CN gain	1	60.00
chr18:49,035,472–49,406,866	371,394	q25.1	CN gain	10	60.00
chr18:55,807,318–55,861,598	54,280	q25.3	CN gain	10	60.00

Region chr:bp start-bp end	Length (bp)	Cytoband	Event	Genes	Frequency (%)
chr18:55,899,795–55,986,610	86,815	q25.3	CN gain	2	60.00
chr5:59,367,552–59,417,133	49,581	q32	CN gain	4	60.00
chr5:67,518,696–67,532,344	13,648	q33	CN gain	3	60.00
chr5:81,157,085–81,374,416	217,331	q35	CN gain	0	60.00
chr1:117,087,221–117,377,134	289,913	q37	CN gain	13	60.00
chr6:48,348,336–48,987,554	639,218	q23.1	CN loss	0	60.00
chr8:76,368,492–76,582,392	213,900	q33.3	CN loss	9	60.00

Table 3

Proposed genes involved in canine oral melanoma pathogenesis

Proposed gene	Cell function
CFA 30 gain	
SLC27A2	Lipid biosynthesis and fatty acid degradation.
HDC	Converts L-histidine to histamine, associated with HDC include mast cell neoplasm.
GABPB1	Transcription factor.
USP8	Required for the cell to enter the S phase of the cell cycle. Also functions as a positive regulator in the Hedgehog signaling pathway in development and downstream signaling of activated FGFR.
TRPM7	Kinase activity is essential for the ion channel function.
SPPL2A	Member of the GXGD family of aspartic proteases.
CFA 30 Loss	
SPRED1	Tyrosine kinase substrate that inhibits growth-factor-mediated activation of MAP kinase through C-KIT receptor signaling pathway.
RASGRP1	Diacylglycerol (DAG)-regulated nucleotide exchange factor specifically activating RAS through the exchange of bound GDP for GTP, which activates the Erk/MAP kinase cascade.
FAM98B	Component of the tRNA-splicing ligase complex
CFA 3 loss	
FGFR3	Tyrosine-protein kinase that plays an essential role in the regulation of cell proliferation, differentiation, and apoptosis
TACC3	Motor spindle protein that may play a role in stabilization of the mitotic spindle. This protein may also play a role in growth a differentiation of certain cancer cells.
TMEM129	Multi-pass membrane protein (Potential)
SLBP	Stabilizes mature histone mRNA and could be involved in cell-cycle regulation of histone gene expression.
FAM53A	May play an important role in neural development.

Table 4

Homologous copy number aberrations, gain (*G*) or loss (*L*), between canine (*CFA*) melanocytic lesions, malignant melanoma (*Mel*) and benign melanocytomas (*Ben*) and two human (*HSA*) melanoma subtypes, mucosal melanoma (mucosal), and acral melanoma (acral)

Genes	Region in HSA (Mb)	G/L in mucosal	G/L in acral	Region in CFA (Mb)	G/L in mel	G/L in ben
CDK4	12q14 (12–57.74)	G	G	15–53	L	N
CDKN2A	9p21 (9–21.96)	L	L	11–44.06	L	N
PTEN	10q32.3 (10–87.86)	L	L	26–40.0	L	L
MYC	8q24.21 (8–127.73)	G	G	13–27.28	G	N
KIT	4q12 (4–75.57)	G	N	13–49.50	G	N
TP53	17p13.1 (17–7.66)	N	N	5–35.0	L/G	L
CCND1	11q13 (11–69.65)	G	G	18–51.1	L	N
RB-1	13q14.2 (13–48.48)	N	N	22–6.0	L	N
CDKN1A	6p21.2 (6–36.68)	G	G	12–8.6	L	N
B-RAF	7q34 (7–140.92)	G	G	16–11.49	L	N

Chromosome Res. Author manuscript; available in PMC 2017 June 07.